Journal of Plant Diseases and Protection (2022) 129:505–520
https://doi.org/10.1007/s41348-022-00570-2

ORIGINAL ARTICLE

Evaluation of the benefits of combined reflection and transmission hyperspectral imaging data through disease detection and quantification in plant–pathogen interactions

Stefan Thomas[1] · Jan Behmann[2] · Uwe Rascher[3] · Anne-Katrin Mahlein[4]

Received: 16 April 2021 / Accepted: 5 January 2022 / Published online: 19 January 2022

Abstract

Previous studies investigating the performance of transmission and reflection datasets for disease detection showed inconsistent results. Within the studies, the performance of transmission imaging varied significantly for the detection of biotroph and necrotrophy plant pathogens, while reflection imaging showed excellent results in both studies. The current study explores the hypothesis that the disparity between these results might be correlated with the different interactions of the respective pathogens with the host plants and the way light interacts with the plant tissue. *Pyrenophora teres* f. *teres* and *Puccinia hordei*—the causative agents of net blotch and brown rust in barley—have been investigated with focus on early-stage detection and quantification (disease severity) of symptoms. Datasets of hyperspectral imaging time-series measurements were analysed through application of multiple data analysis methods (support vector machines; principal component analysis with following distance classifier; spectral decomposition) in order to compare the performance of both datasets for the detection of disease symptoms. It could be shown that transmittance-based brown rust detection (e.g. 12% disease severity) is outperformed by reflectance-based detection (e.g. 36% disease severity) regardless of the algorithm. However, both the detection and quantification of brown rust through transmittance were more accurate than those of powdery mildew in earlier studies. Transmittance and reflectance performed similar for the detection of net blotch disease during the experiments (~ 1% disease severity for reflection and transmission). Each data analysis method outperformed manual rating in terms of disease detection (e.g. 15% disease severity according to manual rating and 36% through support vector machines for rust reflection data). Except for the application of a distance classifier on net blotch transmittance data, it could be shown that pixels, which were classified as symptomatic through the data analysis methods while estimated to represent healthy tissue during manual rating, correlate with areas at the edges of manually detected symptoms. The results of this study support the hypothesis that transmission imaging results are highly correlated with the type of plant–pathogen interaction of the respective pathogens, offering new insights into the nature of transmission-based hyperspectral imaging and its application range.

Keywords *Puccinia hordei* · *Pyrenophora teres* f. *teres* · Data analysis · Disease detection · Hyperspectral imaging · Reflectance · Transmittance

✉ Anne-Katrin Mahlein
Mahlein@ifz-goettingen.de

[1] Department of Phytopathology (360a), Institute of Phytomedicine (360), University of Hohenheim, 70599 Stuttgart, Germany

[2] INRES Plant Disease, University of Bonn, 53115 Bonn, Germany

[3] IBG2: Plant Sciences, Research Centre Jülich, 52428 Jülich, Germany

[4] Institute of Sugar Beet Research (IfZ), 37079 Göttingen, Germany

Introduction

The use of optical sensors for plant phenotyping and detection of both abiotic and biotic stresses has become increasingly common as a research focus (Roitsch et al. 2019; Mahlein et al. 2019; Oerke 2020). However, the overwhelming majority of current studies are focussed on measuring the properties of light which is reflected from the plant tissue in order to correlate changes with plant stress reactions (Kuska et al. 2015; Alisaac et al. 2018; AlSuwaidi et al. 2018). Meanwhile research into the possibilities of the spectral properties of light which has been transmitted through

the plant tissue is rarely conducted (Zhang et al. 2016; Hovi et al. 2018; Sun et al. 2018). Recent studies about the possibilities of transmitted light for plant–pathogen detection with hyperspectral imaging sensors showed inconsistent results.

Thomas et al. (2017) performed a measurement of combined reflection and transmission with focus on plant–pathogen interaction with hyperspectral imaging sensors. The authors investigated barley leaves, which were inoculated with conidia of *Blumeria graminis* f. sp. *hordei*—the causative agent of powdery mildew—with the HyperArt measurement setup (Bergsträsser et al. 2015) for simultaneous measurement of reflection and transmission. The results of the study showed that it is possible to detect powdery mildew infection of barley leaves at leaf level two days before symptoms are visible on RGB images through automatically analysed reflection-based hyperspectral data. Furthermore, it could be shown that the combination of reflection and transmission data was advantageous to distinguish late powdery mildew symptom and spontaneous necrosis of resistant barley leaves. However, the results of the study did show that transmission-based detection of powdery mildew symptoms was not possible before symptoms on the leaves were already visible for two days with reflection-based RGB imagery. These results stood in contrast to the study of Bergsträsser et al. (2015), which performed single measurements of visible symptoms of *Cercospora beticola* infection on sugar beet leaves. It was shown that reflection and transmission-based data performed equally for the detection of disease symptoms. Thomas et al. (2017) theorised that this could be explained based on the different interaction of the two pathogens with the plant tissue. While powdery mildew symptoms, caused by the biotroph pathogen *Blumeria graminis* f. sp. *hordei*, develop as small pustules on the leaf surface with the fungi only penetrating the epidermis cells of the plant (Bhat et al. 2005; Dean et al. 2012), *Cercospora* leaf spot symptoms, caused by the necrotroph pathogen *Cercospora beticola*, appear as necrotic lesions on the leaves once the fungi switches to its necrotic phase after penetrating the leaf tissue through the stomata and spreading intercellularly (Steinkamp et al. 1979; Rangel et al. 2020). In this article, further studies into the matter and principle of transmission measurement via optical sensors are presented in an attempt to confirm the hypothesis of Thomas et al. (2017).

Light interacts with plant leaves in a complex matter. Upon reaching the plant surface (cuticle and epidermis), a significant portion of the light is directly reflected and can be measured, providing information about the plant surface it interacted with (Fig. 1). The portion of the light which is neither reflected nor absorbed by the plant's surface enters the plant tissue, where it is scattered diffusely as it interacts with organelles and intercellular air spaces (Vogelmann et al. 1989). During the passing of the plant tissue, a small amount of light is reflected back to the upper surface, and the majority of light travels through the plant's mesophyll layer and the lower epidermis of the leaf. Upon reaching the surface-air border, the majority of the diffusely scattered light is reflected back into the plant, with only a small portion is being transmitted through the leaf as it arrives at the surface-air border in the right angle (Fig. 1; Brakke 1994). The light, which was reflected, is scattered diffusely once more as it travels back through the plant tissue layers up to the surface-air border of the upper epidermis, where a small portion is being transmitted and measured together with the surface reflection by reflection-based imaging methods, while the larger portion of the light is reflected back into the leaf tissue again (Fig. 1). This complex process allows the plant to maximize the usage of incoming light for photosynthesis (Brakke 1994). These processes provide the reason why it is possible to detect metabolic changes in plants with reflection-based measurement. The study of Nansen (2018) did also show that hyperspectral measurements have a considerable penetration of measured objects. Their study showed that different backgrounds influence leaf measurements—especially with multiple layers of leaves being measured.

This could explain why reflection measurement outperforms transmission measurement for biotroph pathogens like *Blumeria graminis* f. sp. *hordei*, which mostly interact with the plant at the epidermis layer, as direct reflection at the plant surface permits the detection of the fungal tissue. Meanwhile transmitted light would mix with light, which has not interacted with fungal tissue or affected epidermis cells, due to diffuse scattering while traversing the leaf tissue, reducing the detection efficiency. Necrotroph pathogens like *Cercospora beticola* tend to be more invasive in their interaction with the host plant, which would result in a similar detection accuracy to biotroph pathogens in reflectance measurement, but an increased performance in transmittance measurement, as the traversing light, interacts with the pathogen and infected plant tissue in deeper layers of the leaf.

This study aims to provide insights into the matter of transmittance measurements of plant–pathogen interaction through practical experiments with a set of pathogens with diverse lifestyles. Measurements with the HyperArt setup were performed with barley leaves inoculated with pathogens, which interact with different layers of the plant tissue, as time-series measurements.

Puccinia hordei, the causative agent of brown rust, is a biotrophic pathogen, which enters infected barley leaves through the stomata (Fig. 2b; Voegele 2006). Once inside the plant mesophyll, the fungi grows, forming intercellular haustoria to feed upon the plant before finally forming colonies, which break through the epidermis to release new spores (Fig. 2b; Voegele 2006).

Pyrenophora teres f. *teres* (anamorph: *Drechslera teres*), the causative agent of net blotch, is a necrotrophic pathogen.

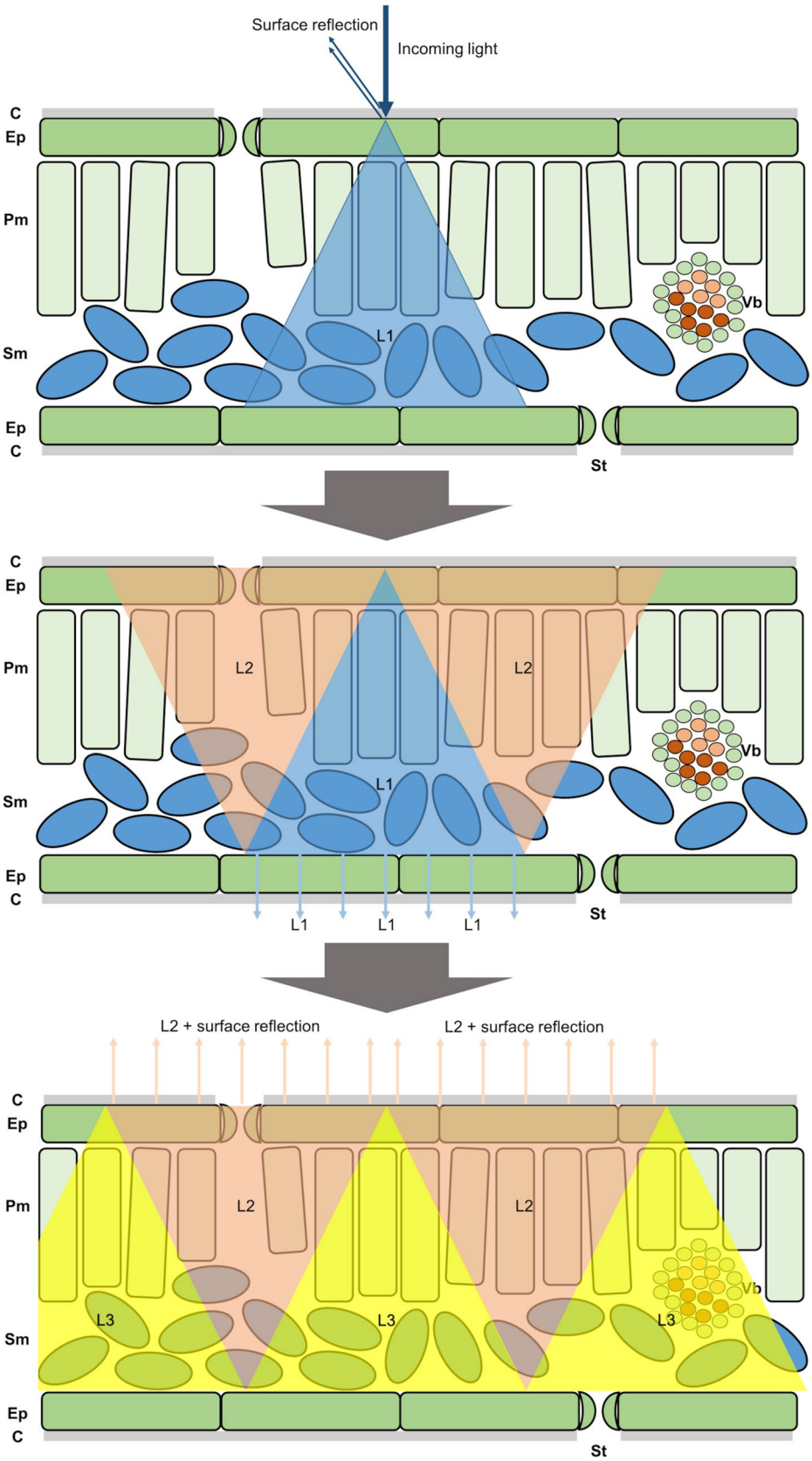

Fig. 1 Pathway of light when interacting with a plant leaf. Upon reaching the plant's surface, a portion of the light is reflected back from the cuticle (C) and epidermis (Ep), while the rest of the light enters the plant tissue in a diffusely scattered manner (L1, blue cone). The light crosses both palisade- (Pm) and spongy mesophyll (Sm)—being partially absorbed and scattered back to the leaf surface as indirect reflection—before reaching the epidermis and cuticle un the bottom of the leaf. Here, a portion of the light is transmitted, thereby exiting the leaf as transmitted light (L1, blue arrows), while the rest is being reflected at the leaf surface-air border and traverses the mesophyll tissue again while being diffusely scattered (L2, orange cones). Upon reaching the epidermis and cuticle of the top of the leaf, a portion of L2 is transmitted as indirect reflection and would be measured with the light coming from the surface reflection, while the rest is reflected from the leaf surface-air border to continue its path through the leaf (L3, yellow cones). St = stomata, Vb = vascular bundle

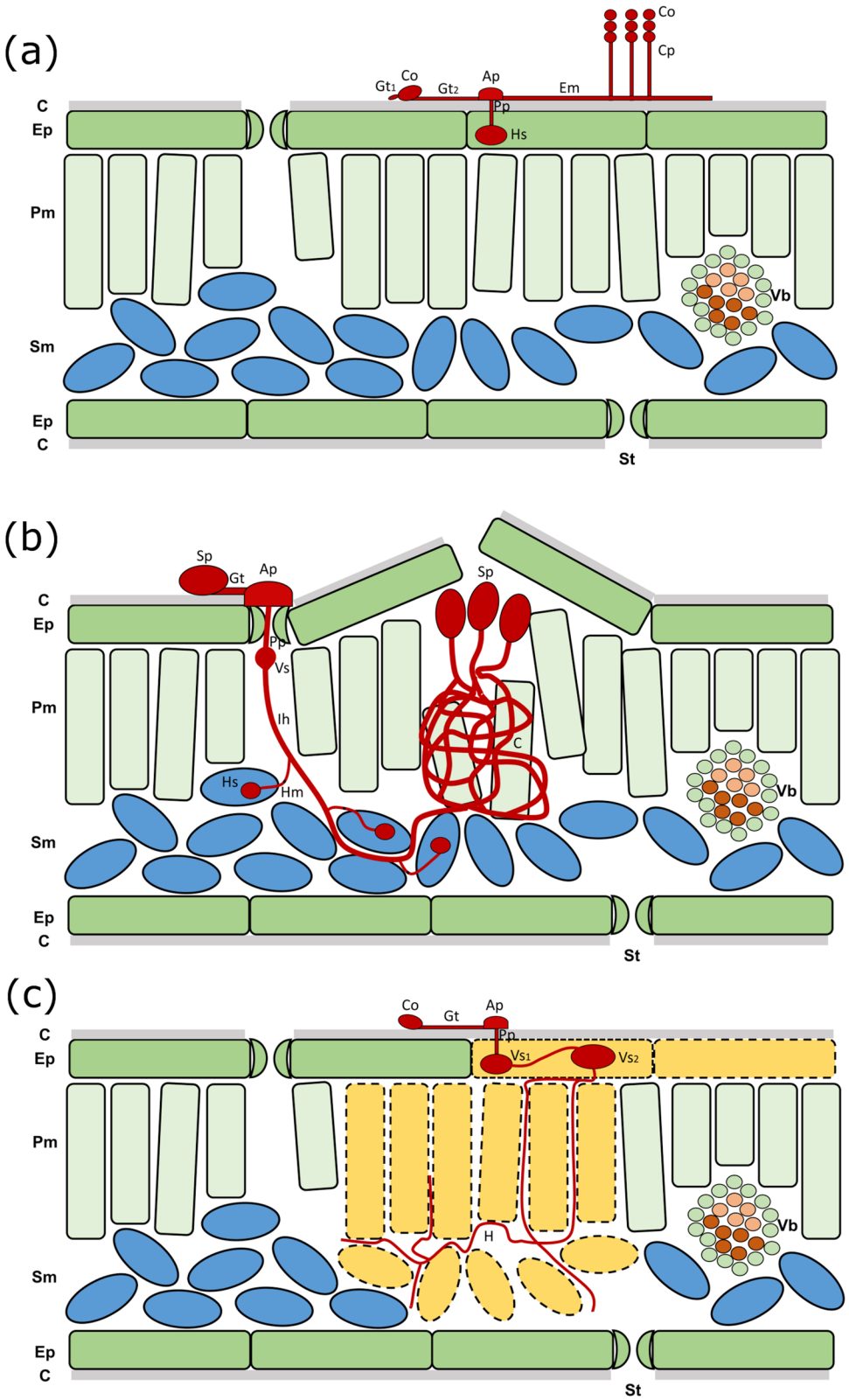

Fig. 2 Interactions of the pathogens *Blumeria graminis* f. sp. *hordei* (**a**), *Puccinia hordei* (**b**) and *Pyrenophora teres* f. *teres* (**c**) with barley leaves. C = cuticle, Ep = epidermis, Pm = palisade mesophyll, Sm = spongy mesophyll, St = stomata, Vb = vascular bundle, Co = conidia, Gt = germination tube, Ap = appressorium, Pp = penetration peg, Hs = haustorium, Em = epiphytic mycelia, Cp = conidiophores, Sp = Spore, Vs = vesicle, Ih = infection hypha, Hm = haustorial mother cell, C = colony, H = hyphae

It penetrates directly through the cuticle, cell wall, and cell membrane of the host plants epidermis cells, where it forms a primary and secondary intracellular vesicle (Fig. 2c; Liu et al. 2011). When the secondary vesicle is formed, the host epidermis cell—as well as nearby epidermis cells—is functionally disrupted. A hypha forms intracellular from the

secondary vesicle and breaks into the intercellular space of the mesophyll, where it secretes toxins/effectors which lead to the disruption of nearby mesophyll cells to provide the necrotrophic fungi with nutrients (Fig. 2c; Liu et al. 2011).

The two pathogens interact in a different way compared to *B. graminis* f. sp. *hordei*. The development of *P. hordei* is relatively subtle at first—before the plant tissue gets disrupted through the fungi breaking through the epidermis. Its growth within the mesophyll should allow for increased detection with transmission-based imaging, due to a reduced effect of the light scattering at pathogenic structures deeper within the leaf tissue. *P. teres* f. *teres* causes rapid cell death, which should result in similar results as the measurement of spontaneous necrosis in the study of Thomas et al. (2017) and should be comparable with the characteristic necrotic lesions in the centre of *Cercospora beticola* symptoms, which were investigated by Bergsträsser et al. (2015).

Through this approach—while taking into account the results of previous articles in regards to performance of reflectance and transmittance datasets—it should be possible to shed light on the performance of transmission imaging based on the differing plant–pathogen interactions of biotroph and necrotrophy pathogens. Multiple data analysis methods (both supervised and unsupervised) have been applied to the respective datasets in order to minimize the potential impact on disease detection accuracy. Thereby, observed differences between the performance of reflection and transmission datasets can be attributed to the different host–pathogen interactions of the investigated diseases. The use of an unsupervised data analysis method and its comparison with the presented supervised methods is especially promising, as it does not rely on training data and thereby can both reduce workload and the potential for human error during data labelling.

Materials and methods

Plant cultivation and pathogen material

Hordeum vulgare L. cv. Ingrid wild type (Hinze et al. 1991) plants were grown in TEKU VQB 7 × 7 × 8 cm pots (Pöppelmann, Lohne, Germany) and filled with commercial substrate (Klasmann-Deilmann GmbH, Geeste, Germany) inside a climate chamber at 20/20 °C (day/night) 60% relative humidity (RH) and day light period of 16 h. At growth stage 12 according to BBCH scale (Hack et al. 1992), the plants were inoculated with the respective pathogens and placed in high humidity environment (> 90%) and indirect lighting conditions for two days to maximize chance of infection before the second leaf of each plant was fixed within a custom plastic frame. Twelve plants were used as healthy control, being inoculated with water, and 12 plants were inoculated with a spore suspension (60,000 spores/ml; spores were collected from infected wheat plants and stored at − 80 °C to be used for inoculation directly after thawing) of *P. hordei* (stored field isolate from the area near Bonn) and 6 plants were inoculated through placement of cut leaves, showing heavy symptoms of *P. teres* f. *teres* infection, gathered around the area of Bonn. The inoculations were performed by spraying the spore suspensions and placing leaf pieces equally over the to be inoculated plant leaves for the two days the plants spend under high humidity conditions.

Hyperspectral imaging measurement

The HyperArt system was used to measure reflection and transmission of the plants simultaneously during the experiment (Bergsträsser et al. 2015; Thomas et al. 2017; Patent nr: DE102012005477). The system was modified according to Thomas et al. (2017). All leaves were measured in the visible and near infrared areas of the electromagnetic spectrum (400–1050 nm) in a daily time-series measurement from 3 days after inoculation (dai) to 9 dai. Measurements at earlier times were not possible, due to the requirement of the fungi to have high humility for infection of barley leaves. The leaves were kept fixated within the custom plastic frames over the entire measurement period to ease comparison of disease development at different images in the time series for data analysis. For each measurement, a 99% reflectance white standard (Spectralon, Labsphere Inc., North Dutton, NH, USA) and a white diffuser lambertian transmission foil (Zenith Polymer® ≈ 50% transmission, SphereOptics GmbH, Uhldingen, Germany) was acquired, before measuring the leaf sample. These measurements served as white references for reflection and transmission images for the image normalization (Bergsträsser et al. 2015). Wavelength-dependent differences in the percentage of the reflected and transmitted light of the two white references were taken into consideration during the normalization process. With each measurement, a dark current image of the internal camera noise was measured by closing an internal camera shutter.

Data analysis

The reflectance and transmittance of the images were calculated by normalising the acquired images over the according white references, serving as standards with known reflection/transmission values, with ENVI 5.1 + IDL 8.3 (ITT Visual Information Solutions, Boulder, CO, USA). The normalized images were smoothened through the application of the Savitzky–Golay filter (Savitzky and Golay 1964) to eliminate noise within the hyperspectral datasets for further analysis. Background masking and separating the hyperspectral

images to single leaves were performed through an automated algorithm (thresholding based on global average). In contrast, the transmission images required manual extraction due to their spectral properties being indistinguishable at places where parts of the frame were covering the plants in order to hold them in place. Due to significant noise within the data at the extremes of the sensor range, the analysed spectral range was reduced to 450–1000 nm.

The collected datasets of reflection- and transmission-based leaf images with developing net blotch and brown rust symptoms, respectively, were analysed with three different data analysis algorithms—support vector machines (SVM, Cortes and Vapnik 1995), spectral decomposition (SD, Keshava and Mustard 2002), and a combination of principal component analysis (PCA) with following distance classifier (DC, Mahalanobis et al. 1996). The SVM represents a supervised approach of data analysis, in which a set of generated training data is used as basis for classification. The SD is an unsupervised method, which generates classes based on distinct datapoints within the analysed dataset. The combination of PCA and DC finally represents a mixed approach of reducing data dimensionality with the unsupervised PCA and sorting the resulting correlation of pixels with the principal components into pre-generated classes with the supervised DC. Classification results of data analysis approaches are investigated in combination with manual rating (MR) to compare the potential of both the reflection and transmission datasets for the characterization and detection of differing plant–pathogen interactions.

In order to prepare the dataset for analysis of its variance with principal component analysis, all spectral signatures were normalized into the unit Euclidian norm to eliminate the influence of non-biologic variance to the measurement. Thereby, the signatures/vectors are treated as points on a high dimensional unit sphere (Dhillon and Modha 2001; Leucker et al. 2016b), capturing the vectors direction while reducing the variance in the dataset. After these preparations, the PCA was performed. PCA is a statistical method which introduced a new axis along the greatest variance into the dataset, thereby transforming it based onto the variance and reducing the data complexity (Wold et al. 1987). The PCAs were performed over the healthy control leaves and the respective inoculated leaves within the dataset, including both reflection and transmission-based images. A supervised classification to determine disease symptoms on the leaves was performed through the application of the DC algorithm (Minimum distance classifier with centroid match method and Euclidian distance) on the results of the PCA. The DC uses a set of training data in order to classify every pixel of the image based on its distance in the Euclidian space from known classes.

An independent analysis of the data was performed by applying a nonlinear support vector machines algorithm on the normalized dataset, which was used for the PCA with following DC. The applied SVM used radial basis function as kernel function to determine linear discriminant functions.

The DC and SVM were both trained with a set of labelled training data, which was generated by an expert, using control- and inoculated leaf images of six healthy and six inoculated leaves, respectively, at 7 dai from rust and net blotch datasets in order to classify both early and late stages of disease symptoms. Each leaf within the dataset averaged between 9000 and 14,000 pixels, with the selected training data for each generated class averaging between 50 and 500 pixels, based on class rarity within the images. The manually annotated data were ordered into 14 classes (brown rust symptoms (early/late, reflection/transmission); net blotch symptoms (early/late, reflection/transmission); healthy tissue (leaf surface1/leaf surface2/leaf vein/leaf tip, reflection; leaf surface1/leaf vein, transmission)) and used as reference within the above classifications. Classes, which referred to healthy plant tissue of their respective datasets, have been combined and are shown as one colour in the result section, due to the focus on disease detection over slight differences in leaf reflection/transmission within different part of the leaf. For the comparison with manual rating and the manual rating itself, the classes were simplified to symptomatic and healthy tissue for their respective datasets, as a precise differentiation for each pixel into different disease stages or via the human eye and without the consultation of spectral signatures for the pixels was not feasible.

Finally, unsupervised spectral decomposition—based on the mixed pixel approach—was used to analyse the datasets. Spectral decomposition factorizes the matrix, which is made up of the to-be analysed hyperspectral dataset, into a canonical form, representing it in terms of its eigenvalues and eigenvectors. This algorithm was applied unsupervised, with the program selecting mixed pixels of the image so as to determine the eigenvalues. The abundance of these eigenvalues within the dataset was then calculated to give out both an abundance map with abundance per pixel, as well as a classification of the image over the generated classes.

The data analysis methods were performed with the FluxTrainer 2.9.0.1 Software (LuxFlux GmbH, Reutlingen, Germany).

Leaves were manually rated by an expert at the end of the experiment 9 dai. The manual rating was performed with a Pseudo-RGB image as basis with the goal to label healthy and infected leaf tissue. Unlike the generated training data, each pixel of the images was sorted into the classes healthy and symptom during this rating to compare disease severity visible by eye with the results of the different data analysis methods. Pixels that showed clearly identifiable disease Symptoms with the bare eye were labelled as Symptom, while other pixels were labelled as healthy.

The results of the manual rating were used as comparison for post classification of the data. This was achieved via a two-ways approach. The leaf images of different dates were compared with each other in order to determine if the classification results which showed pixels as diseased without visible symptoms correlate with symptom development at later dates (Figs. 3 and 4). Furthermore, the classifiers and MR were analysed through confusion matrices of the classification results from the different data analysis methods on both reflection and transmission datasets. Confusion matrices were computed via a C++ program. The results of the confusion matrices were visualized (see Figs. 7 and 8) to determine if the grouping of pixels that was classified as symptomatic in the algorithms but not the MR correlate with the expected development of disease symptoms to further validate the data analysis.

Results

Manual assessment of the gathered datasets

The water-inoculated control plants did not show any development of disease symptoms of either net blotch or brown rust over the course of the experiment.

The plants which were inoculated through direct contact to leaf pieces, infected with *P. teres* f. *teres*, developed net blotch symptoms. First symptoms of the net blotch disease became visible at 5 dai both in reflection- and transmission-based images and slowly progressed until the last measurements were taken at 9 dai (Fig. 3). During this time, the symptoms developed from the initially infected areas of the host plants leaves, which had direct contact with infected leaf parts during inoculation. Throughout the symptom development, the net blotch symptoms proved to be equally visible in reflection and transmission images, showing similar leaf discoloration and symptom area (Fig. 3). During manual rating of the disease severity at 9 dai, the reflection and transmission data were rated with 0.72 and 0.69 percent of the leaf area showing symptomatic tissue, respectively (Table 1).

The plants which were inoculated with *P. hordei* (*Ph*) spore suspension developed without exception brown rust symptoms over the course of the experiment. First disease symptoms became visible at 5 dai in the reflection-based images and 6 dai in the transmission-based images—with the symptoms being easier to distinguish in the reflection-based data (Fig. 4). Symptoms developed over the entire leaf area, starting with discrete, small chlorotic spots at the initial infection sites. Typical yellow, chlorotic areas were forming on the leaves at 5 dai and growing, with brown spore colonies breaking through the epidermis and becoming visible from 7 dai until the end of the experiment—this process could be clearly observed in the reflection-based images (Fig. 4). Meanwhile, in the transmission-based images this process could only be observed as a slight darkening of

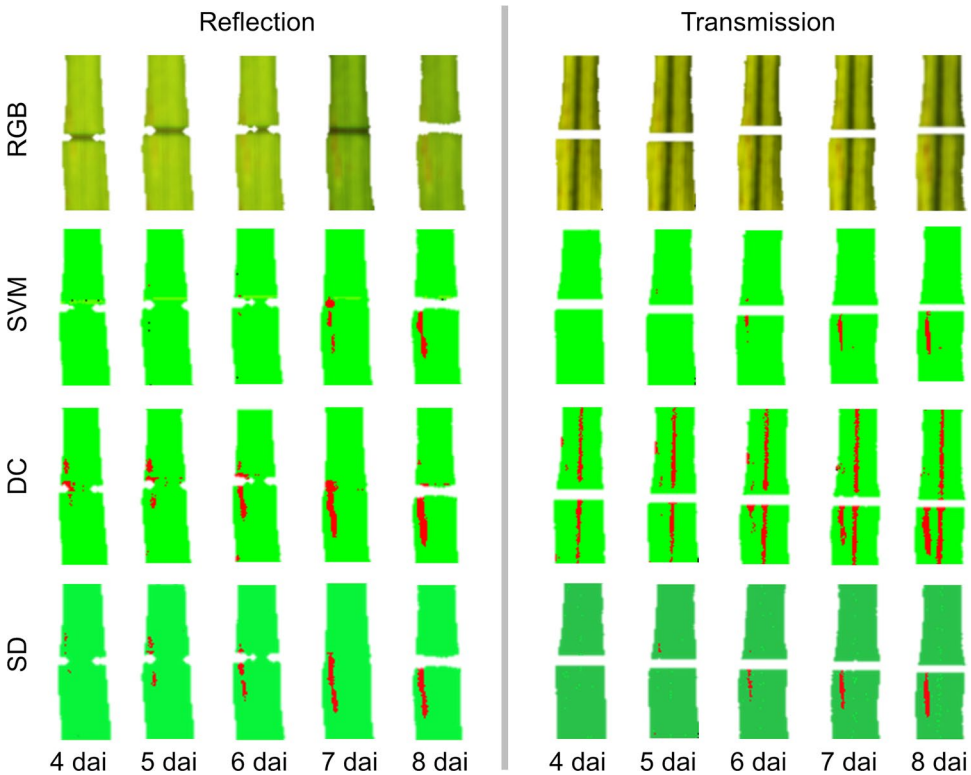

Fig. 3 Reflection and transmission images of an Ingrid wild type leaf, inoculated with *Pyrenophora teres* f. *teres* over the course of the experiment. The Pseudo-RGB images are compared with false colour images, representing the classes healthy (green colours) symptom (red) and artefact (black) of the respective data analysis methods. RGB = Pseudo-RGB, SVM = Support Vector Machines, DC = Distance Classifier, SD = Spectral Decomposition

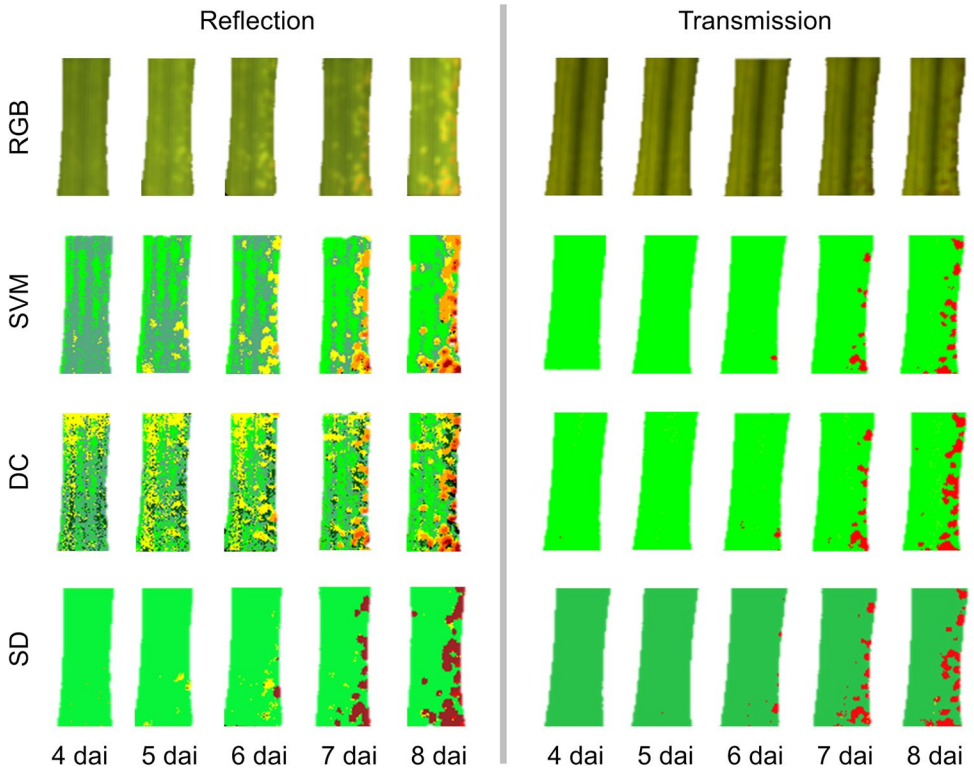

Fig. 4 Reflection and transmission images of an Ingrid wild type leaf, inoculated with *Puccinia hordei* over the course of the experiment. The Pseudo-RGB images are compared with false colour images, representing the classes healthy (green colours) and symptom (yellow and red colours) of the respective data analysis methods. RGB = Pseudo-RGB, SVM = Support Vector Machines, DC = Distance Classifier, SD = Spectral Decomposition

Table 1 Disease severity calculation of net blotch and brown rust inoculated leaves at 9 days after inoculation with different data analysis algorithms and comparison with manual rating

	Net blotch *r* (%)	Net blotch *t* (%)	Brown rust *r* (%)	Brown rust *t* (%)
Manual rating	0.72	0.69	15.25	5.04
SVM	1.04	1.05	35.92	11.72
DC	2.4	11.18	37.9	20.75
SD	1.12	0.98	27.35	13.98

DC, Distance Classifier; SVM, Support Vector Machines; SD, Spectral Decomposition; r, reflectance; t, transmittance

the symptomatic leaf areas, which became visible at 6 dai, and the development of brown spots in the middle of the described darkened areas, starting at 7 dai (Fig. 4). During manual rating of disease severity—based on reflection and transmission datasets—15.25 and 5.04 percent of the leaf tissue were rated as symptomatic tissue, respectively (Table 1).

Analysis of the respective reflection- and transmission-based data through three distinctive data analysis methods

The datasets for the investigated pathogens—for both reflectance and transmittance data—were analysed with the three distinct data analysis methods (SVM, DC, SD), as described above.

The leaf images of the control plants were classified as healthy tissue for both reflectance and transmittance with the exception of < 0.1% of the pixels, which were classified as disease symptoms for SVM and SD classification. The falsely classified pixels were located either at the edge of the leaves or in the areas where the frame was covering parts of the leaves during measurement (Fig. 5). Thereby, containing mixed information of the respective reflected/transmitted light of both the measured leaf and the black background/frame. The DC algorithm—based on the results of the previously performed PCA—performed noticeably worse, having overall the highest tendency to falsely classify pixels in the above-mentioned areas with up to 0.3% of pixels being falsely classified as symptoms. The DC classification also was unable to differentiate between symptoms and the leaf vein in the transmission-based images of the net blotch dataset, causing pixels of the leaf veins to be classified as disease symptom, increasing the falsely classified pixels up to 10% in this specific case (Fig. 5).

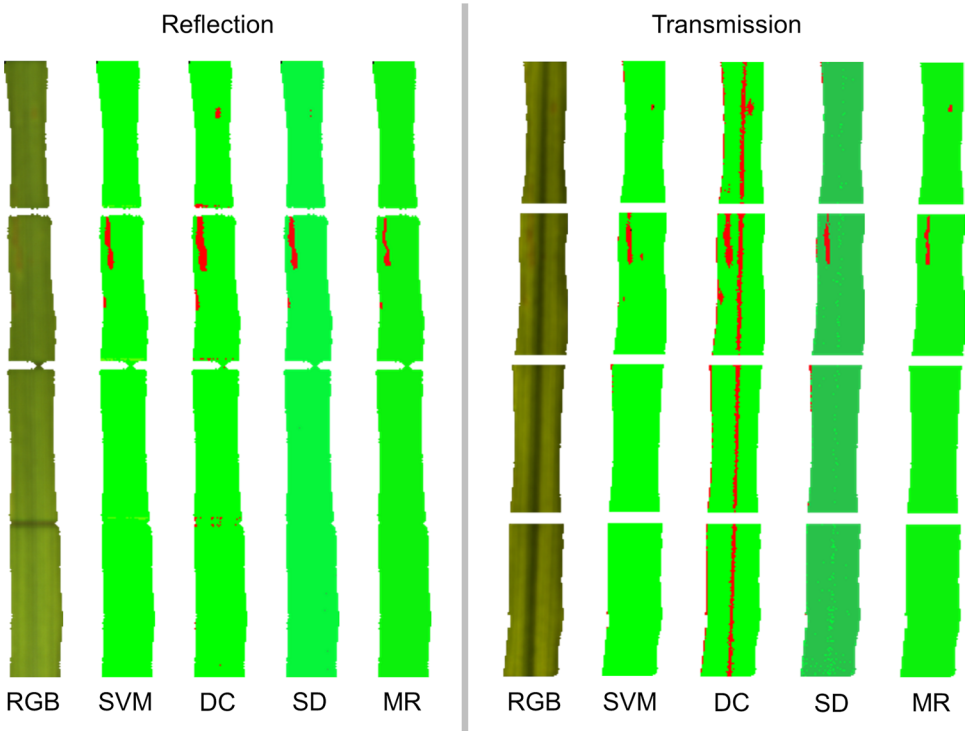

Fig. 5 Reflection and transmission image of an Ingrid wild type leaf, inoculated with *Pyrenophora teres* f. *teres* at 9 days after inoculation. The Pseudo-RGB images are compared with false colour images, representing the classes healthy (green colours), symptom (red), and artefact (black) of the respective data analysis methods, as well as with the results of manual rating of the image by an expert. RGB = Pseudo-RGB, SVM = Support Vector Machines, DC = Distance Classifier, SD = Spectral Decomposition, MR = Manual Rating

Both DC and SD algorithms were able to detect net blotch symptoms within the reflectance images of the inoculated leaves at 4 dai—one day before the symptoms were visible with the human eye—and able to track the development of the symptoms during the following measurement days, whereby the DC did show a clearer detection of early symptoms but was also more prone to misclassify pixels containing healthy tissue as symptoms (Fig. 3). For transmission-based images, the algorithms were able to detect first net blotch symptoms at 5 dai, showing a slightly reduced performance in early disease detection compared to reflectance-based data (Fig. 3). The SVM-based classification performed notably worse for early detection in reflection-based images. Despite using the same training data set as the DC, first symptoms were only detected at 7 dai. Meanwhile, the transmittance images allowed a detection of the symptoms at 5 dai, performing similar to the other two algorithms (Fig. 3).

At 9 dai, the final measurement day for the experiment, net blotch symptoms could be classified by all three data analysis methods in both reflectance and transmittance images, correlating with the results of manual labelling of disease symptoms—both in disease severity (Table 1) and location of disease symptoms on the leaf (Fig. 5). A notable exception being the DC algorithm for the transmission-based image, as the above-mentioned classification error of the leaf vein persists, causing a disparity of about 10% in disease severity compared to manual rating results and other methods.

When looking in more detail at the classification of the specific pixels within the images through the application of confusion matrices with the manual rating serving as the standard method for comparison of the different classification results with classic disease detection approaches. In order to achieve this, one leaf for ach pathogens was manually rated, with the leaf for brown rust consisting of 13,048 and the one for net blotch of 13,418 manually annotated pixels. The results show, that all three algorithms have a high accuracy for the correct classification of healthy tissue and symptoms within the reflection data (89.6% for SVM and 84.5% for SD), with the DC algorithm outperforming the other two for disease detection (100%; Table 2). Within the transmission dataset, the accuracy of all three algorithms is reduced (78.4% for SVM, 70.1% for SD and 97.9% for DC), with DC showing an uncharacteristically high error margin for misclassification of healthy tissue (10.6%) due to the misclassification of pixels showing the leaf vein as symptoms (Table 2).

Within the brown rust dataset, the SVM classified first pixels in reflectance images as disease symptoms at 4 dai, one day before the disease became visible with the human eye and classifies symptomatic leaf areas correctly over the course of the experiment (Fig. 4). In the transmission-based images, the SVM only detects disease symptoms at 6 dai. Due to high difficulties in differentiating early disease symptoms and healthy tissue, it was, however, necessary to create multiple classes of healthy leaf tissue within the training data for both SVM and DC. As wheat leaves are

Table 2 Results of confusion matrix on images classified with manual rating compared to the applied data analysis methods for net blotch and brown rust infected leaves at 9 days after inoculation

	Manual rating			
	Net blotch		Brown rust	
	Healthy (%)	Symptom (%)	Healthy (%)	Symptom (%)
Reflection				
SVM				
Healthy	99.6	0.4	74.2	25.8
Symptom	10.4	89.6	3	97
DC				
Healthy	98.3	1.7	69.6	30.4
Symptom	0	100	13.7	86.3
SD				
Healthy	99.4	0.6	83.5	16.5
Symptom	15.5	84.5	11.7	88.3
Transmission				
SVM				
Healthy	99.5	0.5	92.2	7.8
Symptom	21.6	78.4	14	86
DC				
Healthy	89.4	10.6	84.1	15.9
Symptom	2.1	97.9	4.5	95.5
SD				
Healthy	99.5	0.5	90.2	9.8
Symptom	29.9	70.1	7.7	92.3

Values in percent represent the percentage of the total amount of pixels within the respective classes, which were classified correctly based on the results of the manual rating

DC, Distance Classifier; SVM, Support Vector Machines; SD, Spectral Decomposition

not entirely homologous in their reflection and transmission properties—based on leaf age, leaf structures, leaf angle, etc.—and the early pathogen signatures being similar to those of the control leaves multiple distinct classes at different pathogen stages and at healthy leaf areas with specific features have been created. This explains the early misclassification of pixels showing healthy leaf tissue as disease symptoms at 4 dai for the DC (Fig. 4). As shown in Fig. 4, the DC classification increases in accuracy over the course of the experiment, correlating significantly better with the results of the other data analysis methods at 8 and 9 dai (36/12% for SVM reflectance/transmittance, 38/21% for DC reflectance /transmittance). When applied to the transmittance images, the DC does not have these issues, accurately detecting disease symptoms from 6 dai onwards like the SVM. The transmission-based dataset could be classified with only a single class for healthy tissue, showing a more uniform spectral signature over the leaf area when compared with the reflectance dataset. Disease symptom detection with the SD classified first disease symptoms at 5 dai and 6 dai for reflectance and transmittance images, respectively, and shows accurate detection over the course of the experiment (Fig. 4), with a slightly reduced disease severity assessment compared to SVM and DC (27/14% for reflectance/transmittance).

Comparison of the classification results at 9 dai shows that all data analysis algorithms achieve significantly higher disease severity ratings then manual rating for both reflectance (e.g. 36% for SVM compared to 15% for manual rating (brown rust)) and transmittance (e.g. 12% for SVM compared to 5% for manual rating (brown rust)) datasets (Table 1), while the spatial distribution of symptomatic pixels within the images matches for data analysis methods and manual rating (Fig. 6).

The post-classification results of the respective confusion matrices show that the selected algorithms are able to accurately detect disease symptoms, which were labelled in the manual rating, in both reflection (97% for SVM, 86.3% for DC, 88.3% for SD) and transmission (86% for SVM, 95.5% for DC, 92.3% for SD) data (Table 2). The detection accuracy of the SVM for reflectance images being notably higher than other algorithms. Both DC and SD have a higher accuracy for transmittance image symptom detection, while the accuracy of the SVM decreases when compared with the results of reflection data. All algorithms classified a high percentage of pixels which did not show clearly visible disease symptoms—and where thereby marked as healthy tissue in the manual rating—as symptoms (25.8% for SVM, 30.4% for DC, 16.5% for SD) for the reflectance images, while the results of the transmittance images show a lower error margin (Table 2).

Discussion

The results of this study show differences within the performance of transmission-based measurement approaches, depending on the way pathogens interact with the host plant. Within this study, the biotroph pathogen *Puccinia hordei* and the necrotroph pathogen *Pyrenophora teres* f. *teres* have been investigated with both reflection and transmission measurement approaches. Combined with the results of Thomas et al. (2017), which investigated the reflection and transmission-based detection of the biotroph pathogen *Blumeria graminis* f. sp. *hordei* and theorized the low performance of transmission data was related to the interactions of light with the tissue while passing the leaf, this allows the estimation of cases in which the addition of transmission-based approaches would be beneficial for increased accuracy in disease detection. B. graminis f. sp. hordei mainly interacts with the epidermis layer of the plant,

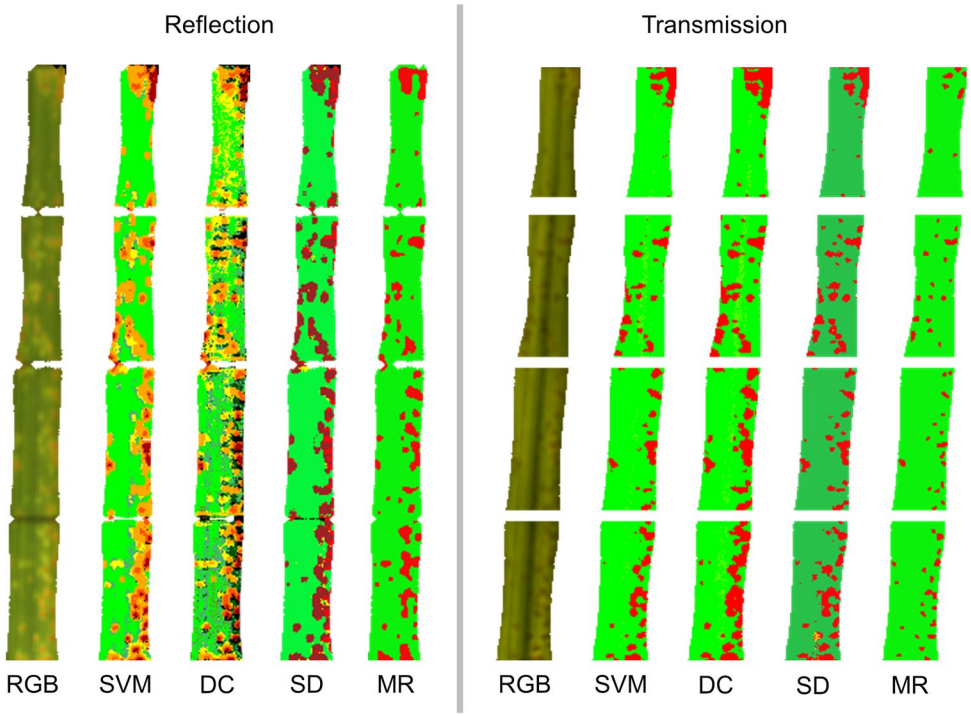

Fig. 6 Reflection and transmission image of an Ingrid wild type leaf, inoculated with *Puccinia hordei* at 9 days after inoculation. The Pseudo-RGB images are compared with false colour images, representing the classes healthy (green colours) and symptom (yellow and red colours) of the respective data analysis methods, as well as with the results of manual rating of the image by an expert. RGB = Pseudo-RGB, SVM = Support Vector Machines, DC = Distance Classifier, SD = Spectral Decomposition, MR = Manual Rating

while *P. hordei*—albeit also a biotroph pathogen—grows into the intercellular space and interacts with cells within the mesophyll layer (Fig. 2). The necrotroph pathogen *P. teres* f. *teres* secretes mycotoxins, which cause necrosis over all layers of the leaf tissue in areas where the mycelium of the pathogen is present (Fig. 2). This study provides insights about the interaction of transmitted light with the different pathogens and thereby its potential for disease detection, based on the performance of transmission measurement for the detection and quantification of the pathogens with their differing host–pathogen interactions and the comparison with reflection-based measurement.

Evaluation of transmission-based imaging data for disease detection

The theory postulated by Thomas et al. (2017) that light scattering within the leaf influences the disease detection through transmittance images and thereby the interactions of pathogens with the host plant play an important role in detection speed and accuracy is supported by the results of the current study.

It could be shown that net blotch symptoms are detected with no substantial differences in disease severity at later stages. This was true for both manual rating of reflectance and transmittance images, as well as classification results with SVM and SD (Table 1). The combination of PCA and DC did classify a notably higher number of pixels in the transmittance data as diseased, and this can be explained due to the inability of the algorithm to discern pixels showing the leaf veins from pixels with disease symptoms (Table 2). Figure 7 shows that the majority of pixels which were classified as showing symptoms in the transmission images of the DC results while being labelled as healthy in the MR align with the leaf vein placement on barley leaves. These results coincide with the findings of Bergsträsser et al. (2015), which investigated the advantages of combined reflectance and transmittance measurements for disease severity estimation on developed *Cercospora* leaf spot symptoms via a comparison of *Cercospora* leaf spot index results derived from reflectance and transmittance images. Like the net blotch disease, which was investigated in this study, *Cercospora* leaf spot disease also causes necrotic lesions on infected sugar beet leaves (Mahlein et al. 2012; Leuker et al. 2016). The results of both studies also correlate with findings of Thomas et al. (2017) that transmission-based images allowed for precise detection of spontaneous necrosis on leaves and their differentiation from late stage powdery mildew symptoms, which required more complex methodology when differentiated through reflection-based data.

In contrast, the estimation of disease severity of brown rust on barley leaves within this study showed that the estimates based on transmittance images were lower compared to reflectance image-based estimates (Table 1). The algorithms did each classify a significant number of pixels, which could not be labelled as symptomatic during the MR, into the symptoms group for both reflectance and transmittance images (Table 2). The location of these pixels shows that they are mostly located at the outer edges of areas which were labelled as symptoms through MR, hinting at

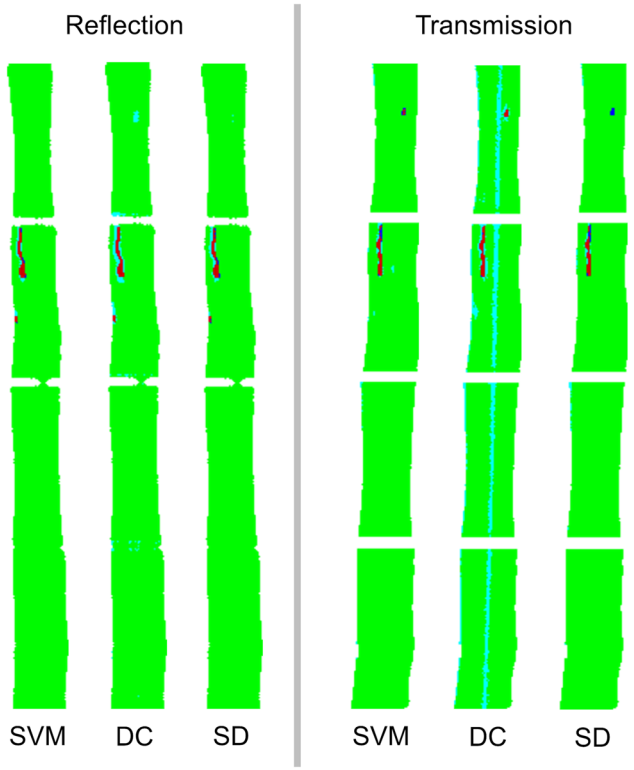

Fig. 7 False colour visual representation of confusion matrix results on net blotch infected leaves at 9 dai for reflection and transmission images. The images show the comparison of the respective data analysis method classification outcome compared to manual rating. Green and red pixels representing healthy and symptom classification which showed no difference for manual rating and classification. Light blue coloured pixels represent pixels which were classified as symptoms in the data analysis and healthy in the manual rating. Dark blue coloured pixels, respectively, represent pixels that were labelled as symptoms in the manual rating and classified as healthy through the data analysis. SVM = Support Vector Machines, DC = Distance Classifier, SD = Spectral Decomposition

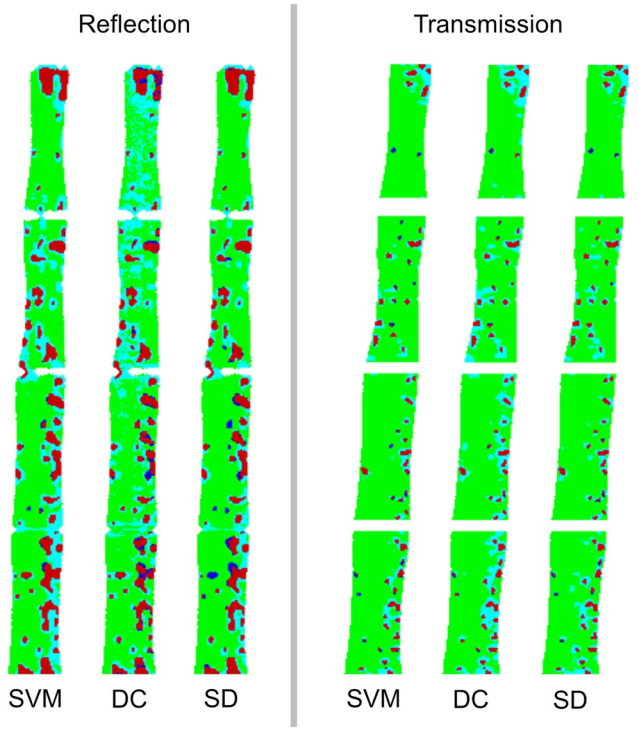

Fig. 8 False colour visual representation of confusion matrix results on brown rust infected leaves at 9 dai for reflection and transmission images. The images show the comparison of the respective data analysis method classification outcome compared to manual rating. Green and red pixels representing healthy and symptom classification which showed no difference for manual rating and classification. Light blue coloured pixels represent pixels which were classified as symptoms in the data analysis and healthy in the manual rating. Dark blue coloured pixels, respectively, represent pixels that were labelled as symptoms in the manual rating and classified as healthy through the data analysis. SVM = Support Vector Machines, DC = Distance Classifier, SD = Spectral Decomposition

the possibility to detect brown rust infection before visible symptoms appear at a given location (Fig. 8). Despite the success of the algorithms for disease detection, it showed that the estimated disease severity in transmission-based images was significantly lower than reflection-based images, with MR and SVM showing the highest discrepancy of about 66% between the results—~15% and ~35% disease severity for reflectance and ~5% and ~11% for transmittance, respectively (Table 1). Visibility of brown rust symptoms with the human eye within the transmittance images was mostly limited to areas where spore colonies had formed and broken through the leaf epidermis, with chlorotic lesions from prior rust development being barely visible once larger areas were infected. Nevertheless, the detection of brown rust symptoms was more accurate and could be earlier detected within transmission-based data and then, the powdery mildew symptoms in the study of Thomas et al. (2017), in which powdery mildew symptoms, were detected through principal component analysis. All used algorithms in the current study have shown to be able to detect disease symptoms one day after they became visible within the reflectance images (Fig. 4) compared to two days for powdery mildew in the previous study (see Thomas et al 2017, Fig. 6).

These findings show, that while pathogen detection through reflectance is similar for biotroph (*B. graminis*) and necrotroph (*C. beticola*) pathogens shown in earlier studies (Bergsträsser et al. 2015; Thomas et al. 2017), the detection efficiency through transmittance varies considerably for pathogens investigated in the current study. Necrotroph pathogens like net blotch (current study) and *Cercospora* leaf spot disease (Bergsträsser et al. 2015) can be detected equally well through reflection and transmission at late disease development stages. Meanwhile, for biotroph pathogens, such as brown rust (current study) and powdery mildew (Thomas et al. 2017), reflection-based

pathogen detection outperforms transmission-based detection. Nevertheless, it could be shown that, when comparing the results of brown rust detection through transmittance data with the detection of powdery mildew symptoms in Thomas et al. (2017), the classification of brown rust symptoms through transmission-based data analysis is more accurate and allows for earlier detection of the pathogen then those for powdery mildew—with transmission imaging being able to detect powdery mildew two days after symptoms could be detected through reflection imaging, while brown rust could be detected with a delay of one day only. These trends can be explained by the interaction of transmitted light with the plant tissue (Fig. 1). As the light becomes diffusely scattered while traversing the leaf tissue, it stands to reason that more intrusive pathogens, which interact with deeper cell layers inside the leaf, would be less affected by these effects, then pathogens which interact with the plant surface and epidermis layers, such as powdery mildew (Fig. 9). As necrotroph pathogens cause significantly more cellular damage than biotroph pathogens and, like the example of net blotch shows (Fig. 2), interact with all layers of the leaf, it is reasonable that they would be best suited for transmission-based detection. These findings support the hypothesis of Thomas et al. (2017) that the differences in transmission-based disease detection for selected pathogens are rooted in the nature of their interaction with the host plant and suggest that transmission-based pathogen

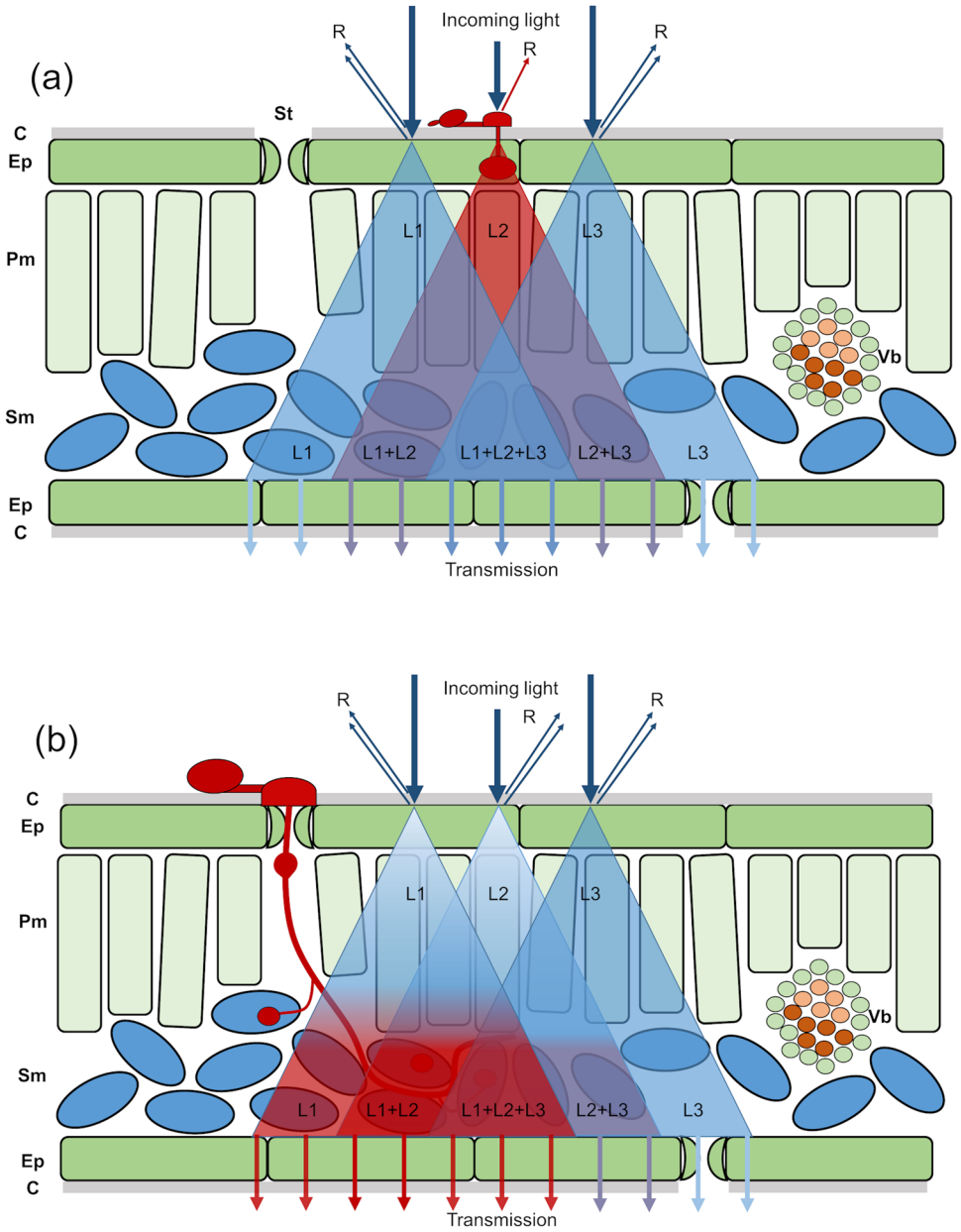

Fig. 9 Influence of diffuse light scattering inside plant leaf tissue for transmission-based measurement of pathogens which interact with the leaf surface and epidermis (Ep). Incoming light is colliding with the cuticle (C) and epidermis of the leaf, where a portion of the light is being directly reflected (R). This leads to a direct interaction of the reflected light with pathogens that grow on the leaf surface, resulting in a significant influence on the reflected lights wavelength. However, the portion of the light which is being transmitted through the leaf is being diffusely scattered (L1, L2, L3). For non-intrusive pathogens like powdery mildew, **a** this leads to a significant overlap of light, which did not come in contact with the pathogen, when exciting the leaf tissue as transmitted light (L1 + L2 + L3). For more intrusive pathogens like brown rust, **b** this effect is significantly reduced, as the light interacts with the pathogen in deeper plant tissue layers, thereby reducing the effect of the scattering on detection accuracy for transmitted light. Pm = palisade mesophyll, Sm = spongy mesophyll, St = stomata, Vb = vascular bundle

detection is correlated significantly with the intrusiveness of a given pathogen during its development inside the host tissue.

Early disease detection through transmission

It has been shown by multiple studies that hyperspectral reflectance imaging sensors are able to detect disease symptoms before symptoms are visible with the human eye (Kuska et al. 2015; Thomas et al. 2017; Behman et al. 2018). So far, this could not be shown for images based on transmission, as studies with time-series measurements that compare the performance of reflectance and transmittance hyperspectral images for early plant disease detection are, to the knowledge of the authors, not available—besides Thomas et al. (2017). Within the study of Thomas et al. (2017), powdery mildew infection could be detected based on transmittance images at 6 dai, two days after detection was possible through the reflectance images and at a point when the disease symptoms were already visible by eye in reflection-based RGB images.

In the current study, both net blotch and brown rust symptoms in transmittance images could be detected one to two days after detection was possible in reflectance images for all applied data analysis methods—with the notable exception of net blotch symptom detection through SVM, which can be explained as the SVM failed to detect symptoms in the reflection-based dataset before 7 dai, while the two other algorithms managed to detect at 4 dai. While this exception shows that under certain circumstances, it is possible to achieve earlier disease symptom detection through transmission-based images, it would be more suited to use an algorithm that performs better for the detection of net blotch symptoms as the symptoms were visible by eye at 5 dai.

From the results of these studies, it can be concluded that transmission-based measurements are not well suited for early disease detection, even from highly invasive pathogens. A possible explanation would be that pathogens like net blotch spread from their entry point at the leaf surface (Fig. 2), which might cause changes within the plants spectral signature to be detected in reflectance images, while the internal light scattering inside the leaves prevents detection of these early plant/pathogen interactions through transmission-based imaging (Fig. 9). While this effect would be reduced for more intrusive pathogens like brown rust and net blotch, it could cause an increase in mixed spectra—containing partial information of symptomatic and healthy leaf areas within a pixel due to internal light scattering—in the transmission data during early pathogen development in transmission measurement compared to reflection measurement.

Comparison of data analysis methods for disease detection and disease severity estimation within this study

Due to the relatively small size of the datasets, which were collected in the experiments, it was decided that—while deep learning approaches have recently shown to be promising in plant stress detection (Golhani et al. 2018; Singh et al. 2018; Feng et al. 2020)—classical machine learning methods would be applied within the current study. While the datasets consist of two independent time series measurements per pathogen, containing 12 and 6 plants, respectively, with thousands of pixels per leaf, it was deemed unlikely that the amount of data would be sufficient for the requirements of deep learning approaches (Singh et al. 2018). Meanwhile machine learning methods have shown excellent results for the analysis of optical data for the estimation of plant parameters in the past, as well as recent studies (Wahabzada et al. 2015; Heckmann et al. 2017; Ugarte Fajardo et al. 2020).

Three different data analysis methods have been used in this study and were compared to MR of the RGB images in order to verify the results of the experiments and minimize the risk that the conclusions are adequate to investigate the characteristics of transmitted light for the investigation of plant–pathogen interactions. In comparison with the MR, every algorithm achieved a higher disease severity estimation for both net blotch (Fig. 5) and brown rust (Fig. 6) symptoms both for reflectance and transmittance images (Table 1). These results, while promising, are posing the question if the classifications of the different algorithms are correct, or misclassifying pixels showing healthy tissue as symptomatic. To clarify this issue, the results of each algorithm were investigated twofold. First, the classification results of images early in the time-series were compared with pseudo-RGB images from later stages for both net blotch (Fig. 3) and brown rust (Fig. 4) datasets. As the leaves were fixed during the entire timeframe of the measurements, it was possible to compare the placement of pixels within different visibility stages. Furthermore, the results of the post-classification through confusion matrices compared to the MR were visualized for both net blotch (Fig. 7) and brown rust (Fig. 8) images at 9 dai. These visualizations show that the vast majority of the pixels which were classified as showing symptoms through the data analysis are grouped around clusters of pixels that were labelled as symptomatic in the MR. It was expected that the different data analysis methods are able to classify pixels without symptoms being visible to the human eye, as it is one of the main interests in analysing hyperspectral imaging data to detect disease symptoms before they are visible by the human eye in RGB images (Behman et al. 2018).

Among the data analysis methods, the combination of PCA and DC showed the highest estimations of disease

severity, but is also the method that has been shown to be most prone to mistakenly classify healthy tissue as symptoms for net blotch (transmission, Fig. 7) and brown rust (reflection, Fig. 8). In these cases, the SVM was able to clearly differentiate between disease symptoms and healthy tissue, while being trained on the same set of training data. The SVM as a supervised method performed well for both early detection and disease severity estimation, with the notable exception of net blotch reflectance images (Fig. 3). The unsupervised SD performed well in all cases, being able to detect symptoms as early as the supervised methods—with the exception of brown rust reflectance, where the SVM was able to detect symptoms one day prior to other methods (Fig. 4)—and was overall the least prone to misclassification. SD has the added advantage that the unsupervised algorithm does not require training data in order to function and did classify disease symptoms and healthy tissue while generating fewer classes, then the supervised methods required. However, the SD had in all cases the lowest disease severity estimates when compared with other algorithms, but still outperformed MR (Table 1).

The combination and comparison of the results of different data analysis algorithms ensured that no false conclusions through performance abnormalities of a single algorithm while investigating the properties of reflectance and transmittance datasets could occur. This was necessary, as it has been shown in earlier studies, that the accuracy of different machine learning methods can vary depending on the investigated dataset (AlSuwaidi et al. 2018; Barreto et al. 2020). While outliers in algorithm performance, such as the late detection of brown rust symptoms in reflectance images of SVM and the misclassification of leaf vein pixels as net blotch symptoms through DC, occurred it was possible to identify them through comparison with the alternative data analysis algorithms employed within the study.

Conclusion

The postulated theory that the nature of the plant–pathogen interaction during pathogen infection is related to the possibility to detect disease symptoms through transmission-based imaging is being supported by the results of this study. Thereby, the use of transmission measurement is most suited for invasive pathogens, which cause tissue damage in deeper layers of the leaf, or in order to separate stress factors which show a high similarity within the changes to the spectral signature of reflectance data. Transmission-based measurements seem to be outperformed by reflection-based measurements in general when it comes to early disease detection.

Supplementary Information The online version contains supplementary material available at https://doi.org/10.1007/s41348-022-00570-2.

Acknowledgements The authors would like to thank the members of the INRES-Plant Protection and Plant Diseases and IBG2: Plant Sciences for their support during the experiments and fruitful discussions. Furthermore, the authors would like to thank the reviewers for helpful comments and constructive critique of the article. Experiments in this study were conducted at the INRES of the University of Bonn, as well as the IGB2: Plant sciences of the Research Centre Jülich as part of the CROP.SENSe.net program.

Author's contributions ST, UR and AKM designed the study and refined the hyperspectral measurement system. ST performed the hyperspectral measurements. ST and JB performed the statistical analysis. ST drafted the manuscript with support from JB, UR and AKM. All authors read and approved the final manuscript.

Funding Funding was provided by the German Federal Ministry of Education and Research (BMBF) within the scope of the competitive grants program "Networks of excellence in agricultural and nutrition research—CROP.SENSe.net" (Funding code: 0315529), junior research group "Hyperspectral phenotyping of resistance reactions of barley," within the German-Plant-Phenotyping Network (project identification number: 031A053), and by the Daimler and Benz foundation. Uwe Rascher and Anne-Katrin Mahlein are partially funded by the Deutsche Forschungsgemeinschaft (DFG, German Research Foundation) under Germany's Excellence Strategy—EXC 2070-390732324.

Data availability The datasets, which were generated and analysed during the study, are not publicly available due to their large sizes. However, they can be provided by the corresponding author upon request.

Code availability Fluxtrainer and Envi software are commercially available. Matlab scripts can be provided by the corresponding author upon request.

Declarations

Conflicts of interest Not applicable.

References

Alisaac E, Behmann J, Kuska MT, Dehne H-W, Mahlein A-K (2018) Hyperspectral quantification of wheat resistance to Fusarium head blight: comparison of two Fusarium species. Eur J Plant Pathol 152:869–884

AlSuwaidi A, Grieve B, Yin H (2018) Feature-ensemble-based novelty detection for analyzing plant hyperspectral datasets. IEEE J Select Top Appl Earth Observ Remote Sens 11:1041–1055

Barreto A, Paulus S, Varrelmann M, Mahlein A-K (2020) Hyperspectral imaging of symptoms induced by *Rhizoctonia solani* in sugar beet: comparison of input data and different machine learning algorithms. J Plant Dis Prot 127:441–451

Behmann J, Bohnenkamp D, Paulus S, Mahlein A-K (2018) Spatial referencing of hyperspectral images for tracing of plant disease symptoms. J Imaging 4:143

Bergsträsser S, Fanourakis D, Schmittgen S, Cendrero-Mateo MP, Jansen M, Scharr H, Rascher U (2015) HyperART: non-invasive quantification of leaf traits using hyperspectral absorption-reflectance-transmittance imaging. Plant Methods 11:1–17

Bhat R, Miklis M, Schmelzer E, Schulze-Lefert P, Panstruga R (2005) Recruitment and interaction dynamics of plant penetration resistance components in a plasma membrane microdomain. Proc Natl

Acad Sci USA 102:3135–3140. https://doi.org/10.1073/pnas.0500012102
Brakke TW (1994) Specular and diffuse components of radiation scattered by leaves. Agric Meteorol 71:283–295
Cortes C, Vapnik V (1995) Support-vector networks. Mach Learn 20:273–297
Dean R, Van Kan JAL, Pretorius ZA, Hammond-Kosack KE, Pietro AD, Spanu PD, Rudd JJ, Dickman M, Kahmann R, Ellis J, Foster GD (2012) The top 10 fungal pathogens in molecular plant pathology. Mol Plant Pathol 13:414–430. https://doi.org/10.1111/j.1364-3703.2011.00783.x
Dhillon IS, Modha DS (2001) Concept decompositions for large sparse text data using clustering. Mach Learn 42:143–175
Feng X, Zhan Y, Wang Q, Yang X, Yu C, Wang H, Tang Z, Jiang D, Peng C, He Y (2020) Hyperspectral imaging combined with machine learning as a tool to obtain high-throughput plant salt-stress phenotyping. Plant J 101:1448–1461
Golhani K, Balasundram SK, Vadamalai G, Pradhan B (2018) A review of neural networks in plant disease detection using hyperspectral data. Inf Process Agric 5:354–371
Hack H et al (1992) Einheitliche codierung der phänologischen entwicklungsstadien mono-und dikotyler pflanzen–erweiterte BBCH-Skala. Allgemein. Nachrichtenbl Deut Pflanzenschutzd 44(12):265–270
Heckmann D, Schluter U, Weber APM (2017) Machine learning techniques for predicting crop photosynthetic capacity from leaf reflectance spectra. Mol Plant 10:878–890
Hinze K, Thompson RD, Ritter E, Salamini F, Schulze-Lefert P (1991) Restriction fragment length polymorphism-mediated targeting of the ml-o resistance locus in barley (Hordeum vulgare). Proc Nat AcadSci 88(9):3691–3695. https://doi.org/10.1073/pnas.88.9.3691
Hovi A, Forsström P, Mõttus M, Rautiainen M (2018) Evaluation of accuracy and practical applicability of methods for measuring leaf reflectance and transmittance spectra. Remote Sens 10(1):25. https://doi.org/10.3390/rs10010025
Keshava N, Mustard JF (2002) Spectral unmixing. IEEE Signal Process Mag 19:44–57
Kuska M, Wahabzada M, Leucker M, Dehne H-W, Kersting K, Oerke EC, Steiner U, Mahlein A-K (2015) Hyperspectral phenotyping on the microscopic scale: towards automated characterization of plant-pathogen interactions. Plant Methods 11:28
Leucker M, Wahabzada M, Kersting K, Peter M, Beyer W, Steiner U, Mahlein A-K, Oerke E-C (2016) Hyperspectral imaging reveals the effects of sugar beet QTLs on *Cercospora* leaf spot resistance. Funct Plant Biol 44:1–9
Liu Z, Ellwood SR, Oliver RP, Friesen TL (2011) *Pyrenophora teres*: profile of an increasingly damaging barley pathogen. Mol Plant Pathol 12:1–19
Mahalanobis A, Vijaya Kumar BVK, Sims SRF (1996) Distance-classifier correlation filters for multiclass target recognition. Appl Opt 35:3127–3133
Mahlein A-K, Steiner U, Hillnhütter C, Dehne H-W, Oerke E-C (2012) Hyperspectral imaging for small-scale analysis of symptoms caused by different sugar beet diseases. Plant Methods 8:3
Mahlein A-K, Kuska M, Thomas S, Wahabzada M, Behmann J, Rascher U, Kersting K (2019) Quantitative and qualitative phenotyping of disease resistance of crops by hyperspectral sensors: seamless interlocking of phytopathology, sensors, and machine learning is needed! Curr Opin Plant Biol 50:156–162
Nansen C (2018) Penetration and scattering—Two optical phenomena to consider when applying proximal remote sensing technologies to object classifications. PLOS ONE 13(10):e0204579. https://doi.org/10.1371/journal.pone.0204579
Oerke EC (2020) Remote sensing of diseases. Annu Rev Phytopathol 58:225–252
Rangel LI, Spanner RE, Ebert MK, Pethybridge SJ, Stukenbrock EH, de Jonge R, Secor GA, Bolton MD (2020) *Cercospora beticola*: the intoxicating lifestyle of the leaf spot pathogen of sugar beet. Mol Plant Pathol 21:1020–1041. https://doi.org/10.1111/mpp.12962
Roitsch T, Cabrera-Bosquet L, Fournier A, Ghamkhar K, Jiménez-Berni J, Pinto F, Ober ES (2019) Review: new sensors and data-driven approaches—a path to next generation phenomics. Plant Sci 282:2–10
Savitzky A, Golay M (1964) Smoothing and differentiation of data by simplified least squares procedures. Anal Chem 36:1627–1639
Singh AK, Ganapathysubramanian B, Sarkar S, Singh A (2018) Deep learning for plant stress phenotyping: trends and future perspectives. Trends Plant Sci 23:883–898
Steinkamp M, Martin S, Hoefert L, Ruppel E (1979) Ultrastructure of lesions produced by Cercospora beticola in leaves of Beta vulgaris. Physiol Plant Pathol 15:13–26
Sun J, Kunnemeyer R, McGlone A, Tomer N (2018) Optical properties of healthy and rotten onion flesh from 700 to 1000 nm. Postharvest Biol Technol 140:1–10
Thomas S, Wahabzada M, Kuska M, Rascher U, Mahlein A-K (2017) Observation of plant–pathogen interaction by simultaneous hyperspectral imaging reflection and transmission measurements. Funct Plant Biol 44:23–34
Ugarte Fajardo J, Bayona Andrade O, Criollo Bonilla R, Cevallos-Cevallos J, Mariduena-Zavala M, Ochoa Donoso D, Vicente Villardón JL (2020) Early detection of black Sigatoka in banana leaves using hyperspectral images. Appl Plant Sci 8:e11383
Voegele RT (2006) *Uromyces fabae*: development, metabolism, and interactions with its host *Vicia faba*. FEMS Microbiol Lett 259:165–173
Vogelmann TC (1989) Penetration of light into plants. Photochem Photobiol 50:895–902
Wahabzada M, Mahlein A-K, Bauckhage C, Steiner U, Oerke E-C, Kersting K (2015) Metro maps of plant disease dynamics—automated mining of differences using hyperspectral images. PLoS ONE 10(1):e0116902. https://doi.org/10.1371/journal.pone.0116902
Wold S, Esbensen K, Geladi P (1987) Principal component analysis. Chemom Intell Lab Syst 2:37–52
Zhang H, Salo D, Kim DM, Komarov S, Tai Y-C, Berezin MY (2016) Penetration depth of photons in biological tissues from hyperspectral imaging in shortwave infrared in transmission and reflection geometries. J Biomed Opt 21:126006